

# BRG1 Loss Predisposes Lung Cancers to Replicative Stress and ATR Dependency

Manav Gupta<sup>1,2,3</sup>, Carla P. Concepcion<sup>4,5</sup>, Caroline G. Fahey<sup>1,2</sup>, Hasmik Keshishian<sup>6</sup>, Arjun Bhutkar<sup>4,5</sup>, Christine F. Brainson<sup>7,8</sup>, Francisco J. Sanchez-Rivera<sup>9</sup>, Patrizia Pessina<sup>1,2</sup>, Jonathan Y. Kim<sup>4,5</sup>, Antoine Simoneau<sup>10,11</sup>, Margherita Paschini<sup>1,2</sup>, Mary C. Beytagh<sup>4,5</sup>, Caroline R. Stancliff<sup>6</sup>, Monica Schenone<sup>6</sup>, D.R. Mani<sup>6</sup>, Chendi Li<sup>12</sup>, Audris Oh<sup>12</sup>, Fei Li<sup>13</sup>, Hai Hu<sup>13</sup>, Angeliki Karatza<sup>13</sup>, Roderick T. Bronson<sup>14</sup>, Alice T. Shaw<sup>12</sup>, Aaron N. Hata<sup>12</sup>, Kwok-Kin Wong<sup>13</sup>, Lee Zou<sup>10,11</sup>, Steven A. Carr<sup>6</sup>, Tyler Jacks<sup>4,5,15</sup>, and Carla F. Kim<sup>1,2,16</sup>



## ABSTRACT

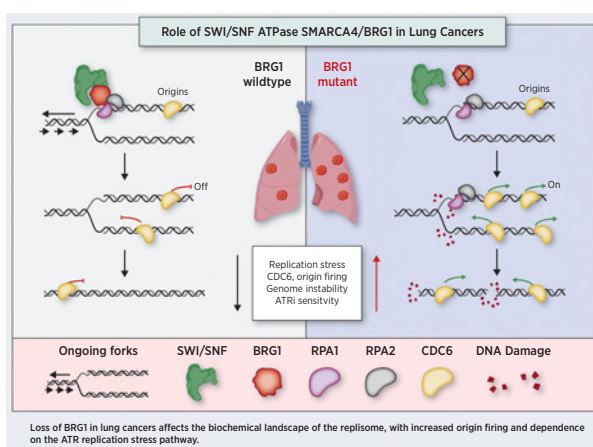
Inactivation of SMARCA4/BRG1, the core ATPase subunit of mammalian SWI/SNF complexes, occurs at very high frequencies in non-small cell lung cancers (NSCLC). There are no targeted therapies for this subset of lung cancers, nor is it known how mutations in *BRG1* contribute to lung cancer progression. Using a combination of gain- and loss-of-function approaches, we demonstrate that deletion of *BRG1* in lung cancer leads to activation of replication stress responses. Single-molecule assessment of replication fork dynamics in *BRG1*-deficient cells revealed increased origin firing mediated by the prelicensing protein, CDC6. Quantitative mass spectrometry and coimmunoprecipitation assays showed that *BRG1*-containing SWI/SNF complexes interact with RPA complexes. Finally, *BRG1*-deficient lung cancers were sensitive to pharmacologic inhibition of ATR. These findings provide novel mechanistic insight into *BRG1*-mutant lung cancers and suggest that their dependency on ATR can be leveraged therapeutically and potentially expanded to *BRG1*-mutant cancers in other tissues.

**Significance:** These findings indicate that inhibition of ATR is a promising therapy for the 10% of non-small cell lung cancer patients harboring mutations in SMARCA4/BRG1.

## Introduction

Lung cancer remains the leading cause of cancer-related mortality worldwide (1). While genotype-specific treatments for EGFR, ROS1, and ALK have transformed the landscape of precision medicine in

**Graphical Abstract:** <http://cancerres.aacrjournals.org/content/canres/80/18/3841/F1.large.jpg>.



patients with lung cancer, the ability to stratify patients has not yet led to targeted therapies for patients whose tumors bear other frequent mutations (2). The mammalian SWI/SNF complexes, also known as *BRG1*/BRM-associated factors (BAF) complexes (referred to hereafter

<sup>1</sup>Stem Cell Program, Division of Hematology/Oncology and Division of Pulmonary Medicine, Boston Children's Hospital, Boston, Massachusetts. <sup>2</sup>Department of Genetics, Harvard Medical School, Boston, Massachusetts. <sup>3</sup>Biological and Biomedical Sciences PhD Program, Harvard University, Boston, Massachusetts. <sup>4</sup>David H. Koch Institute for Integrative Cancer Research, Massachusetts Institute of Technology, Cambridge, Massachusetts. <sup>5</sup>Department of Biology, Massachusetts Institute of Technology, Cambridge, Massachusetts. <sup>6</sup>Broad Institute of MIT and Harvard, Cambridge, Massachusetts. <sup>7</sup>Markey Cancer Center, University of Kentucky, Lexington, Kentucky. <sup>8</sup>Department of Toxicology and Cancer Biology, University of Kentucky, Lexington, Kentucky. <sup>9</sup>Cancer Biology and Genetics Program, Memorial Sloan Kettering Cancer Center, New York, New York. <sup>10</sup>Department of Pathology, Massachusetts General Hospital, Harvard Medical School, Boston, Massachusetts. <sup>11</sup>Massachusetts General Hospital Cancer Center, Harvard Medical School, Charlestown, Massachusetts. <sup>12</sup>Massachusetts General Hospital Harvard Medical School, Boston, Massachusetts. <sup>13</sup>Laura and Isaac Perlmutter Cancer Center, New York University Grossman School of Medicine, NYU Langone Health, New York, New York. <sup>14</sup>Department of Microbiology and Immunobiology, Harvard Medical School, Boston, Massachusetts. <sup>15</sup>Howard Hughes Medical Institute, Cambridge, Massachusetts. <sup>16</sup>Harvard Stem Cell Institute, Cambridge, Massachusetts.

Massachusetts. <sup>15</sup>Howard Hughes Medical Institute, Cambridge, Massachusetts. <sup>16</sup>Harvard Stem Cell Institute, Cambridge, Massachusetts.

**Note:** Supplementary data for this article are available at Cancer Research Online (<http://cancerres.aacrjournals.org/>).

Current address for M. Schenone: Pfizer Cambridge Labs, 1 Portland St, Massachusetts 02139; and current address for A.T. Shaw, Novartis Institutes of Biomedical Research, Cambridge, Massachusetts 02139.

**Corresponding Author:** Carla F. Kim, Boston Children's Hospital, 300 Longwood Ave., Karp 6-211, Boston, MA 02115. Phone: 617-919-4644; Fax: 617-730-4693; E-mail: [carla.kim@childrens.harvard.edu](mailto:carla.kim@childrens.harvard.edu)

Cancer Res 2020;80:3841-54

doi: 10.1158/0008-5472.CAN-20-1744

©2020 American Association for Cancer Research.

as SWI/SNF) are multi-subunit protein complexes that use ATP-dependent processes to mobilize nucleosomes to modulate gene expression and are mutated in many cancer types (3–8). Mutations in *SMARCA4/BRG1*, the ATPase core of SWI/SNF chromatin remodeling complexes, have been found to be prevalent at a high frequency in lung cancer (9–12). Furthermore, the genomic location of *BRG1* on chromosome 19p13.2 along with key lung cancer genes *KEAP1* and *STK11* has been associated with LOH events that compound the cases of *BRG1* mutations with those that sustain whole chromosome arm deletions and subsequent inactivation (13). In a recent study, in which *BRG1* mutations were found in 10% of non-small cell lung cancers (NSCLC), mutations in *BRG1* commonly occurred with other well-known lung cancer mutations in *KRAS* and *TP53* (14). Clinical outcomes in patients with *BRG1*-mutant lung cancer were poor and showed limited efficacy with standard-of-care treatments (14). Thus, the current understanding of this genotype in patients with lung cancer remains limited, from both a mechanistic and a clinical standpoint.

Functionally, monoallelic or biallelic inactivation of *Brg1* during murine embryogenesis leads to tumors or preimplantation lethality, respectively, but certain tissue types including the lung acquire frequent *BRG1* mutations during tumorigenesis (15). Moreover, targeted deletion of *Brg1* in carcinogen-induced lung cancer models has been shown to enhance lung cancer progression and promote metastasis (16, 17). Also notable is the fact that, genetically engineered murine models of lung adenocarcinoma spontaneously show loss of *Brg1* focal regions as one of the foremost changes to the murine lung adenocarcinoma progression landscape (18). At the molecular level, the presence of *Brg1* in murine embryonic stem cells promoted decatenation of newly replicated sister chromatids to allow for faithful replication through mitosis (19). This function was dependent on the ability of *Brg1* to recruit topoisomerases to resolve torsional stress in entangled DNA. In murine fibroblasts, loss of *Brg1* resulted in aberrant mitosis, linked to its chromatin modifying properties of heterochromatin states (20). Biochemical interactions between *Brg1* and *Topbp1* were recovered in murine fetal liver cells, suggesting roles for *Brg1* during S-phase (21). In *BRG1*-deficient cancer lines, loss of biochemical interactions between *BRG1* and *Rb* has been linked to uncontrolled proliferation mediated by increased expression of E2F target genes (22). Thus, whereas studies have implicated *BRG1* as either a transcriptional regulator during G<sub>1</sub>-S-phase or as a substrate that promotes specific interactions through mitosis, the effects of *BRG1* loss on DNA replication during cancer progression are unknown. In this study, we sought to address unanswered questions about the mechanistic implications of *BRG1* loss-of-function in lung cancers that could be clinically relevant.

## Materials and Methods

### Human cell lines

Human lung cancer cell lines used in this study include H460, H2009, Calu6, H441, Sw1573, Calu3, HCC827, Calu1, H520, A549, H522, H2030, H1299, H2126, and H157. All cell lines were maintained in RPMI1640 Media (Invitrogen, 11875-119) with 10% FBS (Thermo Fisher Scientific, 35-016-CV), 4 mmol/L L-glutamine (Life Technologies, 25030-164), and penicillin/streptomycin (Life Technologies, 15140122) at 37°C, 5% CO<sub>2</sub>. Cell lines were obtained from the Meyerson laboratory. Cell cultures were routinely tested for and were negative for *Mycoplasma*. Frozen stocks were made for all cell lines and experiments were performed within first few passages after each thaw. *KRAS*-mutant lung adenocarcinoma patient-derived xenograft (PDX)-derived cell lines were provided by the Hata laboratory.

### Murine cell lines and gene editing

Polyclonal *Kras/p53* cell lines (23) generated from C57BL/6J mice (The Jackson Laboratory) were used for the generation of isogenic *Brg1* knockout lines. Cell lines were nucleofected with pX458 (24) vector encoding Cas9, GFP, and a guide against the tomato gene (25) or *Brg1*. Cells were sorted to single cells in a 96-well plate after gating on GFP-positive cells. Clones were expanded and screened by Western blotting for *Brg1* expression. Lines with reduced expression were then sequenced confirmed by Topo cloning.

### Human cell lines and gene editing

Selected guides, *sgTom* control and *sgBRG1*, were cloned into the pLentiCRISPR vector (26), which was used to produce lentivirus using established protocols (27). H460, H2009, and Calu6 were infected and after puromycin selection, single-cell clones were generated and verified by Western blotting. Clones with *BRG1* loss were then sequenced confirmed by Topo cloning. Guide sequences were: *sgTom* ccactgatctcgaactcgtggcc; *sgBRG1* ccactgtggagtgagggaagatcc; and *sgBrg1* ccactgtggagtgaggcaagatcc. The *BRG1* overexpression plasmid (#19148) from the Massague laboratory (28) was purchased through Addgene. For *BRG1* overexpression experiments, retroviruses were generated and packaged in PlatE cells using established protocols (29). Cell lines were infected with viral containing supernatant containing 8 µg/mL Polybrene (Sigma, TR-1003-G) for a period of 10–18 hours. Infected cultures were selected with Hygromycin (Invitrogen, 10687-010) 5 days after infection.

### Drugs

The following drugs were used: DMSO (Sigma, D2438-5X10ML), KU-60019 (Selleck, KU-60019), MK-8776 (Selleck, S2735), irinotecan (Selleck, S2217), olaparib (Selleck, S1060), VX-680 (Selleck, S1048), palbociclib (Selleck, S1116), VX-970 (Cayman Chemical Co., 24198), and hydroxyurea (Sigma, H8627-5G). Pemetrexed and carboplatin were provided by the Wong laboratory.

### Cytotoxicity assays

Cell viability assays were performed with CellTiter Glo (Promega, G7572), as described previously (30). For human dose-dependent experiments, the following doses were used: 0, 0.1, 0.3, 0.5, 0.7, 1, 3, 5, 7, 10, and 50 µmol/L and for murine experiments VX-970 was used at: 0, 0.1, 0.5, 1, 5, and 10 µmol/L. Combination experiments with irinotecan and hydroxyurea were performed at 1 µmol/L and 1 mmol/L, respectively. Following 72 hours of incubation, CellTiter Glo was added per well for 10–15 minutes and ATP-based luminescence was measured on a BioTek Plate Reader. Data were averaged over triplicates and normalized to control (DMSO/water)-treated wells. Log (IC<sub>50</sub>) and SEM values were compared using GraphPad Prism software, and *P* values reported were the sum-of-squares F-statistics.

### Cell cycle

Cell-cycle profiles of human cell lines were determined by bromodeoxyuridine (BrdU) pulse followed by flow cytometry analysis for BrdU/7-AAD-positive cycling cells. Briefly, cells were pulsed with 10 µmol/L BrdU for 1–2 hours, and followed by overnight fixation in 100% ethanol. Cells were stained with BrdU-FITC (BD556028) and 7-AAD for DNA and analyzed by flow cytometry. Murine cell-cycle profiles were determined using the APC BrdU Flow Kit (BD552598) as per the manufacturer's instructions. Asynchronous cell-cycle experiments were performed as described before. All flow cytometry analyses were performed on the BD Fortessa Machine. Data were

subsequently analyzed on FlowJo software and S-phase lengths were determined on the basis of peak intensity of EdU staining at appropriate timepoint.

#### Western blot analysis

Protein was taken from whole-cell extracts made in RIPA buffer (0.5% deoxycholate, 1% CA630, 0.1% sodium dodecyl sulphate, 150 mmol/L NaCl, and 50 mmol/L Tris-8.1). Samples were quantified using the Pierce 660 nm Protein Assay Kit (Thermo Fisher Scientific, 22662). Each sample was denatured in 2× Laemmli Buffer (Bio-Rad, 1610737) at 95°C for 10 minutes. Samples were run on a 4%–15% polyacrylamide gel (Bio-Rad, 456-1086) and transferred onto a nitrocellulose membrane (GE Healthcare, 45-004-003) via wet transfer for 1 hour. Membranes were incubated overnight at 4°C in primary antibody. Anti-HRP (Santa Cruz Biotechnology) secondary antibodies were diluted 1:2,000. ECL-based methods (Perkin Elmer, NEL103001EA) were used to visualize the KODAK BioMax XAR film (Sigma, Z370371-50EA). The following antibodies were used in this study. Cell Signaling Technology antibodies: ATR (2790S), pATR (58014), CHK1 (2360S), pCHK1 (2341S), Histone H3 (4499S), BAF155 (11956S), BAF170 (12760S), ARID1A (12354S), CDC6 (3387T), ORC1 (4731T), RPA1 (2267S), RPA2 (52448S), BAF47 (91735S), LKB1 (3047S), and KEAP1 (8047S). TOPBP1 was purchased from Bethyl Laboratories (8047S).

#### Immunoprecipitation

Cell pellets were washed in cold 1× PBS and resuspended in 50/100 μL RIPA buffer (0.5% deoxycholate, 1% CA630, 0.1% sodium dodecyl sulphate, 150 mmol/L NaCl, and 50 mmol/L Tris-8.1) with Protease (Roche, 11836170001) and Phosphatase Inhibitors (Thermo Fisher Scientific, PIA32957). The samples were lysed on ice for 30 minutes, vortexed every 10 minutes. The lysates were then centrifuged for 30 minutes at 4°C at 14,000 × g. Lysates (100–200 μg) were precleared with specific antibody for 25 minutes by rotation at 4°C. Protein A Agarose Beads (Thermo Fisher Scientific, 10001D) were washed three times in 1 mL RIPA buffer. Approximately 70 μL of beads were added to each protein–antibody sample and rotated overnight at 4°C. Samples were then spun down at 2,300 × g for 2 minutes, washed with 1 mL RIPA buffer, and rotated for 3 minutes at 4°C three times, followed by Western blotting.

#### RNA sequencing

Bulk RNA-sequencing (RNA-seq) was performed in triplicates for murine isogenic cells. Bulk RNA-seq reads that passed quality metrics were mapped to the annotated UCSC mm9 mouse genome build (genome.ucsc.edu) using RSEM (v1.2.12; deweylab.github.io/RSEM; ref. 31) using RSEM's default Bowtie (v1.0.1) alignment program (32). RSEM estimated read counts were used to perform pairwise differential gene expression analysis between experimental conditions using EBSeq (33) with median-by-ratio normalization (34). Mouse gene symbols were updated to their most recent nomenclature using data from the Mouse Genome Informatics (MGI) batch query utility (www.informatics.jax.org/batch) and subsequently mapped to orthologous human gene symbols using mouse-human ortholog assignments (www.informatics.jax.org/downloads/reports/index.html) from MGI (35). Ranked gene lists by fold change were analyzed through a preranked gene set enrichment analysis algorithm against gene ontology (GO) and Reactome databases using MsigDB (36, 37), using default conditions. Normalized enrichment scores (“enrichment score”) for GO categories and Reactome pathways were used to generate dot plots.

#### Kaplan–Meier plots

Survival analysis in patients with lung cancer was performed on Kaplan–Meier plotter (<https://kmplot.com/analysis/>; ref. 38). Kaplan–Meier survival analyses were implemented for patients with NSCLC [lung adenocarcinoma,  $n = 866$  and lung squamous cell carcinoma (LSCC),  $n = 675$ ] using median gene expression values to split patient group. Cox regression analysis was performed to compute HRs with 95% confidence intervals and log-rank  $P$  values. Survival differences between the two risk groups were assessed using the Mantel–Haenszel log-rank test.

#### Xenografts

A total of  $1 \times 10^6$  cells were injected subcutaneously into the flanks of 8- to 12-week-old female Foxn1nu/Foxn1nu mice (The Jackson Laboratory) in a 1:1 ratio with Matrigel. Each mouse received either BRG1 wild-type or knockout cells on the right and left flank, respectively. Following the establishment of visible tumors, mice were randomized for treatment studies. VX-970 was administered from day 7 to 14 at a dose of 60 mg/kg/day in 5% DMSO + 45% PEG300 (Sigma, 57668-5G) + H<sub>2</sub>O once per day for 5 consecutive days by oral gavage. Treatments lasted between 25 and 30 days. Tumor growth was measured every 4 days by caliper in a nonblinded fashion. Subcutaneous tumor volumes were calculated according to the following formula: volume (mm<sup>3</sup>) =  $(l \times b \times h) \times (\pi/6)$ , where  $l$  is the largest dimension followed by  $b$  and  $h$ . All mouse experiments performed at Boston Children's Hospital (Boston, MA) were approved by the Animal Care and Use Committee accredited by the Association for Assessment and Accreditation of Laboratory Animal Care and were performed in accordance with relevant institutional and national guidelines and regulations.

#### Immunofluorescence

Cells were prefixed in 4% paraformaldehyde and antigen unmasking was performed using Citrate Buffer (Thermo Fisher Scientific, TA-250-PM1X). Cells were blocked in 10% donkey serum in 0.2% Triton X-100 in PBS and probed with primary antibodies overnight at 4°C. Following washes and incubation with secondary antibodies, slides were mounted using Prolong Gold with DAPI (Life Technologies, P36935). Images were taken with a Nikon 90i Camera and NIS-Elements software. For γH2AX and RPA2 experiments, cells were preextracted with 0.1% Triton X-100 in PBS for 2 minutes on ice before fixation. For DNA fibers, fiber slides were treated with 2.5 mol/L HCl for 30 minutes and blocked in 3% BSA/PBST (PBS + 0.05% Tween20) for 1 hour. Primary antibody incubation was performed for 1 hour with anti-CldU (Novus, NB 500-169, 1:100) and anti-IdU (BD-347580, 1:20). Following three washes with PBS, fibers were stained with appropriate secondary antibodies for 30 minutes and finally washed, dried, and mounted with Prolong Gold without DAPI (Life Technologies, P36934). Slides were dried overnight at room temperature in the dark, and then stored at 4°C until imaging.

#### Comets

Alkaline comet electrophoresis was performed on the basis of the manufacturer's instructions (Trevigen). Briefly, cells were trypsinized, collected in cold 1× PBS, and mixed in 1:10 ratio with low melting Agarose (Bio-Rad 1613111). Cells/agarose (30 μL) were pipetted and spread gently on a comet slide (Trevigen, 4252-200-01). Following a 10-minute incubation in the dark at 4°C, the comet slides were submerged in Lysis Solution (Trevigen, 4250-050-01) for overnight incubation at 4°C in the dark. The next day, the slides were incubated in alkali unwinding solution for 60 minutes at 4°C and run in an

electrophoresis unit at 17 volts for 34 minutes. Following washes with 70% ethanol and distilled water, slides were allowed to naturally dry in a 37°C incubator, before proceeding to staining with SyBr Gold Nucleic Acid Stain (Thermo Fisher Scientific, S11494).

#### DNA fibers

DNA fibers were performed in accordance to published protocols (39). Briefly, cells were sequentially pulsed with 50  $\mu\text{mol/L}$  CldU (Sigma, C6891) and 100  $\mu\text{mol/L}$  IdU (Sigma, 17125) with PBS washes in between. Cells were then trypsinized and resuspended at a dilution of  $1 \times 10^6$  cells per mL. A total of 2.5  $\mu\text{L}$  were pipetted on the top of a glass slide. Following an approximate 4-minute incubation, 7.5  $\mu\text{L}$  spreading buffer (0.5% SDS, 200 mmol/L Tris-HCl pH 7.4, 50 mmol/L EDTA, and water) was mixed with the cells and allowed to incubate for 2 minutes. Three glass slides were made per condition per experiment. Slides were tilted at 15 degrees to allow DNA fibers to evenly spread on the glass slide. Following that, the fibers were air dried and then fixed in 3:1 methanol:acetic acid solution. Fixed slides were allowed to dry for 20 minutes and then stored at 4°C until immunofluorescence. Measurement of replication structures was performed using ImageJ. A total of 150–200 definitively resolved fibers were quantified per condition per replicate and the percentage of each specific replication structure was calculated on the basis of total counts observed.

#### Mass spectrometry

Murine isogenic cells were scraped in ice-cold PBS, washed twice, and lysed with mild lysis buffer (150 mmol/L NaCl, 50 mmol/L Tris, pH 7.5, and 1% IGEPAL-CA-630 with protease inhibitors) on ice for 30 minutes. Lysates were treated with MNase with calcium chloride for 4 minutes at 28°C. MNase digestion was halted with EGTA. Lysates were then spun at top speed at 4°C using a microcentrifuge, followed by protein quantification through BCA. Samples were diluted with lysis buffer to 1 mg/mL. Antibody (anti-BAF47 or isotype control, 60  $\mu\text{g}$ ) was added to 1 mg of lysate (two process replicates per condition) and incubated overnight at 4°C, rotating. The following day, Protein G Beads (Life Technologies, 10003D) were washed with lysis buffer, resuspended with lysate, and rotated at 4°C for 4 hours. Beads were then washed three times with wash buffer (150 mmol/L NaCl and 50 mmol/L Tris, pH 7.5 with protease inhibitors) and submitted for proteomics analysis. Sample processing for mass spectrometry analysis was performed as described previously (40). Briefly, on-bead digestion of samples was performed for 1 hour followed by elution of samples from the beads, reduction, alkylation, and overnight digestion of the supernatant with trypsin. Digested peptides were labeled using eight channels of tandem mass tag (TMT) 10-plex reagent, mixed, and fractionated on stage tips packed with strong cation exchange disks. Resulting six fractions were analyzed by nanoflow LC/MS-MS on Q-Exactive Plus Mass Spectrometer (Thermo Fisher Scientific) coupled with EASY-nLC 1200 System (Thermo Fisher Scientific). Data were analyzed on Spectrum Mill Proteomics Workbench (Agilent Technologies) using Mus Musculus (mouse) database containing 46,516 entries and downloaded from Uniprot.org on December 28, 2017. The output of Spectrum Mill analysis was a protein level summary table using “subgroup specific top” settings whereby quantitative information of shared peptides between the subgroups of each group was used for quantitation of only the top subgroup, and remaining subgroups used ratios of only subgroup-specific unique peptides to derive protein quantitation values. Statistical analysis was performed using TMT reporter ion ratios of each channel to the median of all channels for all the proteins identified with two or more peptides. Ratios were median normalized aligning the data from the IgG samples separately from the Baf47 samples because the amount of proteins

pulled down by IgG was much less than the Baf47. Linear model analysis was used to compare isogenic wild-type versus mutant samples as described previously (40).

#### Human patient data

The Cancer Genome Atlas (TCGA), PanCancer Atlas patient data were obtained from cBioPortal (41, 42). For transcriptomic analysis of wild-type versus mutant patients, differential expression analysis on the basis of normalized mRNA expression, RSEM (batch normalized from Illumina HiSeq\_RNASeqV2) was retrieved from cBioPortal. For patients with lung adenocarcinoma, all up- and downregulated genes with  $q$  values adjusted by the Benjamini–Hochberg procedure less than 0.05 were classified as differentially expressed. Identical  $q$  value cutoffs were used for downstream analysis of endometrial and stomach carcinoma datasets. GO and cancer pathways’ analysis using differentially expressed genes were performed using the Panther database (43, 44). Genes with  $P < 0.05$ , FDR  $< 0.05$  cutoffs were selected, and gene enrichment ratios were calculated. Gene ratio (“enrichment ratio”) based on total genes represented in each pathway was used to generate dot plots. Correlation analysis was performed on lung TCGA data, using the lung cancer explorer portal (ref. 45; <http://lce.biohpc.swmed.edu/lungcancer/index.php>). For siRNA-knockdown studies in Project DRIVE (<https://oncologyinbr.shinyapps.io/drive/>), ATR RSA scores for topmost and bottommost 50 cancer cell lines were tabulated. Cell line genotypes were obtained from published studies using DEPMAP (<https://depmap.org/portal/>). Similar analysis was performed for CRISPR loss-of-function screens in cancer cell lines from Project ACHILLES. CRISPR Avana 20Q1 datasets were downloaded from DEPMAP. ATR and BRG1 gene’s essentiality were assessed in all lung ( $n = 102$ ) and uterine ( $n = 22$ ) cancer cell lines. Cell lines with BRG1 CERES scores less than  $-0.70$  were filtered to account for cell lines where BRG1 might be essential.

#### Data availability

The RNA-seq data related to isogenic murine Brg1 wild-type and knockout cells have been deposited in the NCBI’s Gene Expression Omnibus (GEO) and is accessible through GEO series accession number GSE154266 (<https://www.ncbi.nlm.nih.gov/geo/query/acc.cgi?acc=GSE154266>). The original Baf47 mass spectrometry data in murine isogenic Brg1 wild-type and knockout cells along with the protein sequence databases used for searches have been deposited in the public proteomics repository MassIVE (<https://massive.ucsd.edu>) and is accessible through MassIVE accession number MSV000085701 (<ftp://massive.ucsd.edu/MSV000085701/>).

#### Statistical analysis and reproducibility

GraphPad PRISM 8, R software, and Tableau were used for statistical and visual analyses. Sample size and error bars are reported in the figure legends. Exact  $P$  values are shown where possible. Unless otherwise noted, statistical tests were performed using unpaired two-tailed Student  $t$  test. The number of times experiments were performed with similar results is indicated in each legend.  $P$  values less than 0.05 were considered significant.

## Results

To identify possible BRG1-dependent functions in lung cancer, we analyzed transcriptomic profiles in patients with lung adenocarcinoma from TCGA, PanCancer cohorts (46, 47). Upregulated genes in BRG1-mutant lung adenocarcinoma predominantly belonged to GO categories associated with DNA replication, elongation, and chromatin remodeling at the centromere (Fig 1A; Supplementary Table S1).

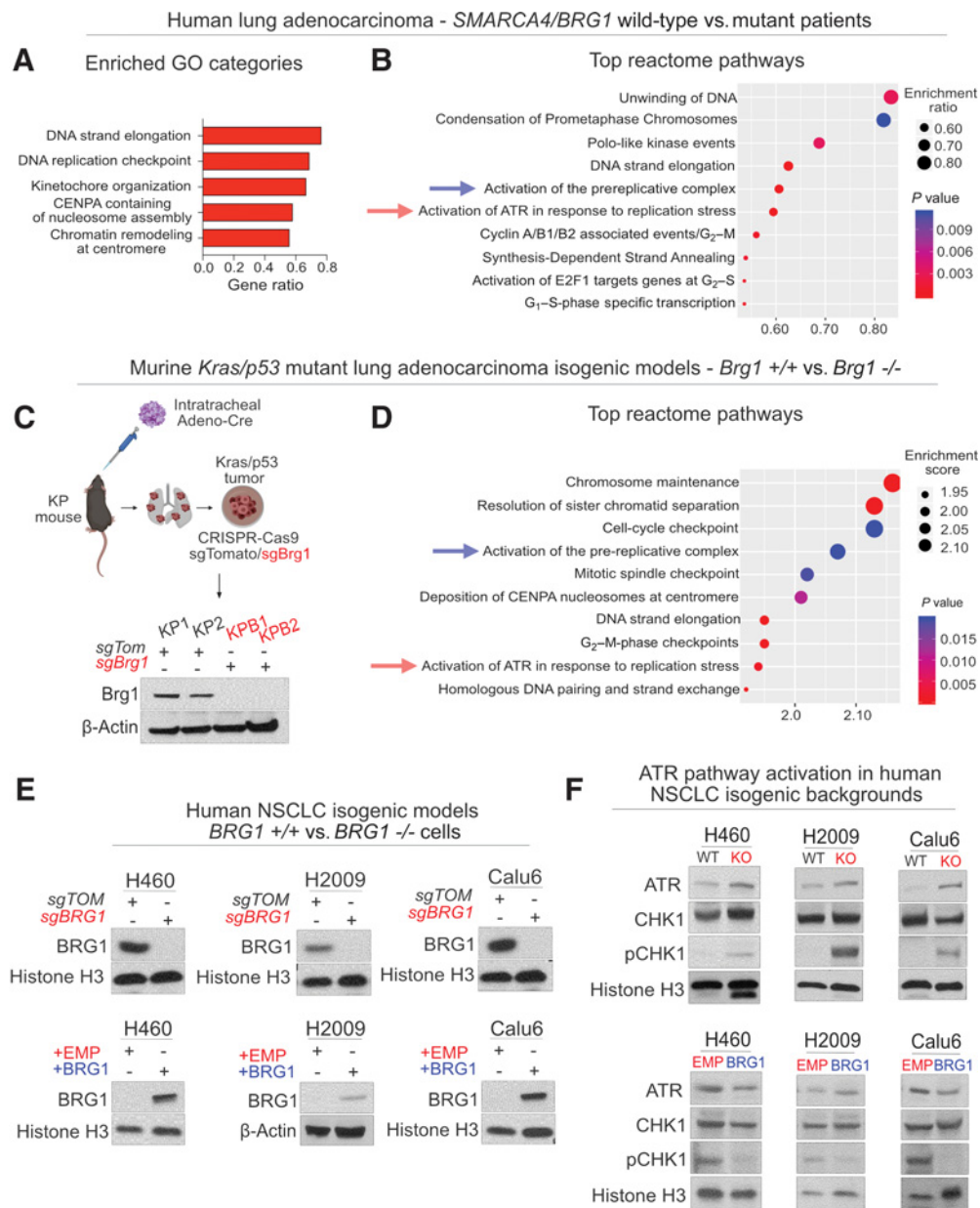


**Figure 1.**

Mutations in *BRG1* correlate with increased prereplication- and ATR-related gene signatures in lung cancers. **A**, GO analysis of upregulated genes in 51 human patients with *BRG1*-mutant lung adenocarcinoma versus 503 *BRG1* wild-type. **B**, Dot plot of top cancer pathways enriched in *BRG1*-mutant lung adenocarcinoma. Arrows, pathways of interest. **C**, Top, schematic of *Brg1* gene editing in KP mouse lung adenocarcinoma cells. Bottom, *Brg1* Western blot analysis. **D**, Dot plot of top cancer pathways in isogenic murine lung adenocarcinoma *Brg1* knockout cells. **E**, Western blot analysis in human isogenic models of *BRG1* loss. **F**, Western blot analysis of ATR activity in human isogenic models of *BRG1* loss.

Analysis of top upregulated cancer Reactome pathways revealed the presence of gene signatures connected to prereplication and activation of the ATR pathway in response to replication stress (Fig. 1B; Supplementary Fig. S1A; Supplementary Table S1). To rule out effects due to background mutations in patient samples, we utilized the *Kras*<sup>G12D/+</sup>; *Tp53*<sup>fl/fl</sup> (*p53*) (KP) murine model of lung adenocarcinoma. This model has been shown to recapitulate key features of KRAS-driven human lung adenocarcinoma in several studies (48, 49). We used CRISPR-Cas9-mediated genome editing with single guide

RNAs targeting either *Brg1* or *tdTomato* to develop isogenic KP-derived lung adenocarcinoma cell lines (KP) that led to loss of *Brg1* protein (Fig. 1C; *n* = 2 lines per genotype). RNA-seq in isogenic *Brg1* wild-type and knockout cells showed enrichment of DNA replication and replication initiation-related GO categories (Supplementary Fig. S1B; Supplementary Table S2). Strikingly, the pathways of prereplication and ATR activation identified in *BRG1*-mutant patient samples were also among the top upregulated pathways in an isogenic setting of *Brg1* loss (Fig. 1D; Supplementary Table S2). We evaluated

the two pathways for overlapping genes that were significantly upregulated in both human and murine lung adenocarcinoma and discovered a set of genes strongly linked to early DNA replication and origin firing (i.e., CDC6, CDC7, and ORC1 among others; Supplementary Fig. S1C). Expression levels of these genes in TCGA lung adenocarcinoma data positively correlated with each other and negatively with *BRG1* expression (Supplementary Fig. S1D). To assess whether a replication stress-related gene signature would inform future clinical relevance, we combined genes identified in the ATR-related pathway from Fig. 1B and D with a comprehensive list of genes discovered to be critical for this process (Supplementary Table S3; ref. 50). We found that high expression of replication stress-related genes correlated with worse survival in patients with lung adenocarcinoma but not LSCC (Supplementary Fig. S1E). These results suggested that *BRG1* loss leads to clinically relevant gene expression changes related to replication stress and prereplication functions.

The presence of increased ATR-related replication stress gene signatures in human and murine lung adenocarcinoma prompted us to measure whether components of the ATR pathway were altered upon *BRG1* loss. To study the effects of *BRG1* loss in human lung cancers, we engineered isogenic *BRG1* wild-type and knockout cell lines using CRISPR-Cas9 genome editing in various NSCLC backgrounds (H460, H2009, and Calu6;  $n = 3$  lines per genotype; Fig. 1E). Reintroduction of *BRG1* in *BRG1*-deficient isogenic cell lines rescued expression of *BRG1* (Fig. 1E). Expression levels of core components of the mammalian SWI/SNF complexes including BAF155 and BAF170 were unchanged upon genome editing of *BRG1* (Supplementary Fig. S1F). ARID1A levels were undetectable in H460 (frameshift mutation), while H2009 and Calu6 showed little to no change between isogenic cell lines. The paralog of *BRG1*, *BRM*, is present in SWI/SNF complexes in a mutually exclusive manner and has been documented to compensate for *BRG1* loss (51). *BRM* protein levels had minimal or no change in H460 and H2009 isogenic cells, whereas Calu6 knockout cells had reduced levels (Supplementary Fig. S1F). *BRM* gene expression levels were reduced in patients with *BRG1*-mutant lung adenocarcinoma compared with that of *BRG1* wild-type patients (Supplementary Fig. S1G). To rule out effects due to changes in LKB1 and KEAP1, we confirmed unchanged levels of these proteins in all isogenic models of *BRG1* loss (Supplementary Fig. S1H and S1I). The integrity of the replication fork is protected, in part, by an ATR-CHK1-dependent signaling cascade, which is essential for fork stabilization and cell viability (52, 53). We found that loss of *BRG1* leads to upregulation of ATR and the activation of the ATR pathway, as measured by phospho-CHK1(Ser345) levels (Fig. 1F). In *BRG1*-rescued isogenic cells, phospho-CHK1 levels were reduced in a *BRG1*-dependent fashion (Fig. 1F). These data support the hypothesis that loss of *BRG1* promotes replication stress-related changes, leading to activation of ATR-mediated responses.

We next sought to understand how *BRG1*-deficient cells trigger a replication stress response using single-molecule DNA fiber spreading to assess fork dynamics (39, 54, 55). It is well established that deregulated fork speed is linked to replicative stress in cells (56). Ongoing forks were identified by red-green tracks (Fig. 2A). While *BRG1* deficiency did not confer proliferative advantages in lung cancer cells (Supplementary Fig. S2A and S2B), there was a significant reduction in fork speed in *BRG1*-deficient cells compared with isogenic controls (~1.5-fold; Fig. 2B and C). Reconstitution with full length *BRG1* increased fork speeds; *BRG1* knockout rescue cells (+*BRG1*) exhibited a significant increase in fork speeds compared

with control *BRG1* knockout cells (+EMP; Fig. 2D and E). To explore cell-cycle changes upon *BRG1* loss, we analyzed asynchronously cycling isogenic cell lines. As with proliferation indices, there was no significant impact of *BRG1* loss on cell-cycle phases across all our models (Supplementary Fig. S2C and S2D). For some isogenic pairs, *BRG1*-deficient lines had more cells in S-phase, which prompted us to examine S-phase lengths (Supplementary Fig. S2C and S2D). EdU pulse-chase experiments (57) showed delays in the completion of S-phases in *BRG1*-deficient cells (Supplementary Fig. S2E). Consistent with this, the expression of G<sub>1</sub>-S-phase- and S-phase-related cyclin/CDK genes was increased in patients with *BRG1*-mutant lung adenocarcinoma (Supplementary Fig. S2F). To measure whether *BRG1*-deficient cells harbor efforts to overcome this increase in replication stress, we used qRT-PCR to analyze gene expression for genes associated with replication fork reversal (i.e., *BLM*, *WRN*, *BRCA1*, *BRAC2*, and *RAD51*) and found overall increased gene expression patterns (Supplementary Fig. S2G). These data suggest that lung cancer cells with *BRG1* loss have replication fork defects, leading to problems in the proper completion of DNA replication.

Next, we tested whether replication stress resulting from *BRG1* deficiency undermines genome integrity. We analyzed  $\gamma$ H2AX staining patterns to represent less damaged (<5 foci/cell), more damaged DNA (>5 foci/cell), and replication stress-associated levels (pan-nuclear expression/cell). Detection of  $\gamma$ H2AX by immunofluorescence showed a significant increase in the percentage of cells harboring pan-nuclear and high number of  $\gamma$ H2AX foci after *BRG1* knockout compared with isogenic controls (Fig. 2F and G). Alkaline single-cell comet analysis further confirmed that loss of *BRG1* is sufficient to induce DNA damage (Fig. 2H and I). Increased DNA damage is consistent with the observations that *BRG1*-mutant lung cancers have higher mutational burdens compared with other common onco- and tumor suppressors in the lung (46, 47, 58, 59). RPA complexes are linked to the stabilization of ssDNA intermediates to allow for efficient replication and ATR activation (52, 53). RPA foci were assessed similarly as described for  $\gamma$ H2AX. A higher proportion of cells with pan-nuclear RPA2 and high number of foci were found in *BRG1*-deficient cells (Fig. 2J and K). This indicated the presence of increased amounts of RPA-bound ssDNA, a canonical substrate for the activation of the ATR pathway, in *BRG1*-deficient cells. Overall, these experiments demonstrate that replication stress and related chromosomal instabilities are major features of *BRG1*-deficient lung cancer cells.

Next, to uncover differences in replication dynamics in lung cancers due to *BRG1* loss, we evaluated the abundance of ongoing replication intermediates through the visualization of DNA fibers (Fig. 3A). Analysis of fiber structures revealed a 2- to 3-fold increase in green-red-green tracks representative of bidirectional activation of new origins of replication in *BRG1*-deficient cells (Fig. 3B-D). Interestingly, there was no change in numbers of stalled forks. (Fig. 3B-D; Supplementary Fig. S3A). At the molecular level, replication origins in eukaryotic DNA are identified by the formation of a prelicensing complex comprised of ORC1-6, CDC6, CDT1, and MCM2-7 proteins. Following prelicensing complex assembly in G<sub>1</sub>-phase, origins are activated through S-phase kinases to initiate the duplication of DNA (60, 61). The presence of deregulated origin firing has been previously shown to promote fork replication defects and increase chromosomal breakage (62). Restoring *BRG1* levels, however, was sufficient to reduce the presence of new origins of replication to control levels (Fig. 3E-G). Both RNA (Supplementary Fig. S3B and S3C) and protein (Fig. 3H and I) levels of essential prelicensing proteins, including CDC6, were upregulated in *BRG1*-deficient cells

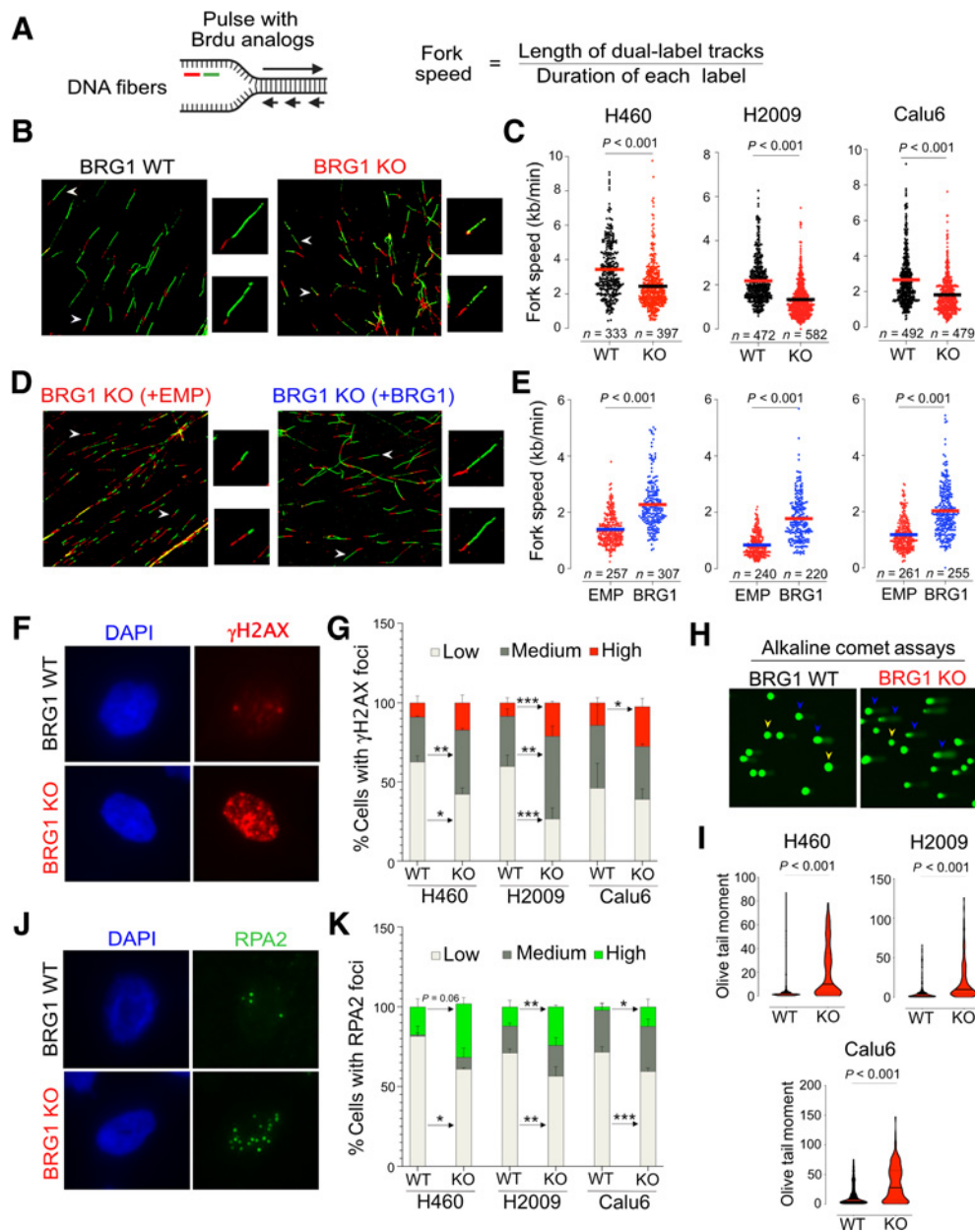


**Figure 2.**

Human isogenic lung cancer cells acquire replication stress and genome instability upon BRG1 deletion. **A**, Schematic of DNA fibers labeling strategy. **B–E**, Representative ongoing DNA fibers in human isogenic models of BRG1 loss (**B** and **C**) and overexpression (**D** and **E**). Insets show individual fibers (white arrowheads;  $n = 2–3$  for each cell line). **F** and **G**, Immunofluorescence show representative  $\gamma$ H2AX foci formation and count analysis in human isogenic models of BRG1 loss ( $n = 2–3$  for each cell line). **H** and **I**, Comet analysis in human isogenic models of BRG1 loss. Yellow arrowheads indicate relatively undamaged nuclei, whereas blue arrowheads indicate relatively higher damaged nuclei ( $n = 3–4$  for each cell line). **J** and **K**, Immunofluorescence shows representative RPA2 foci formation and count analysis in human isogenic models of BRG1 loss ( $n = 2–3$  for each cell line). All images to scale, and all data are mean  $\pm$  SD. \*,  $P < 0.05$ ; \*\*,  $P < 0.01$ ; \*\*\*,  $P < 0.005$ . KO, knockout; WT, wild-type.

and in human patients with BRG1-mutant lung adenocarcinoma. High CDC6 expression also correlated with poor survival in patients with lung adenocarcinoma (Supplementary Fig. S3D). ORC1 was heterogeneously expressed in human isogenic models (Fig. 3H and I). BRG1 expression negatively correlated with prereplication-related gene expression (Supplementary Fig. S3E). Rescue of BRG1 in BRG1-deficient cells lowered overall levels of CDC6, suggesting specific

transcriptomic regulation between BRG1 and origin firing (Fig. 3H and I). Analysis of PDX cell lines recapitulated prereplication defects observed in the human isogenic models (Supplementary Fig. S3F). These data suggest that the replication stress related to the loss of BRG1 in lung cancers could be a consequence of excessive and uncontrolled origin firing and fork response mechanisms, albeit at the cost of increasing amounts of chromosomal instability.

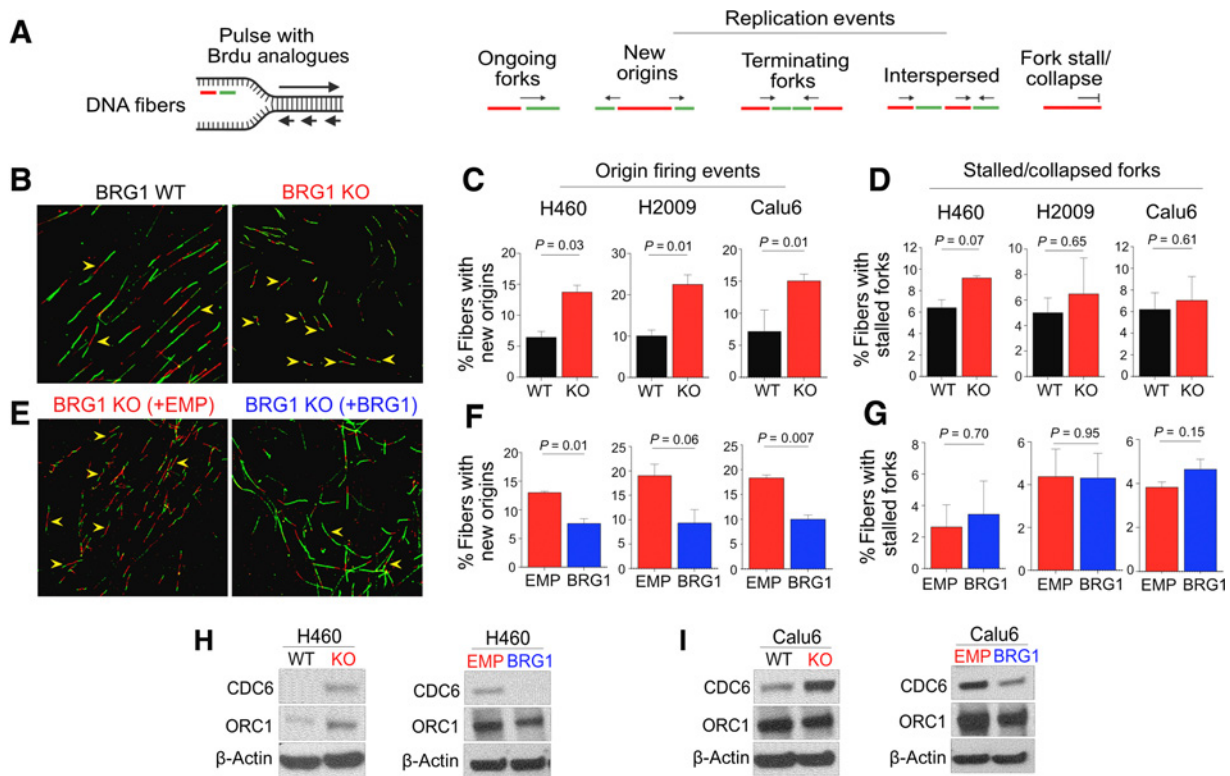


**Figure 3.**

Analysis of ongoing DNA fibers implicate defects in prereplication upon loss of SWI/SNF complex activity. **A**, Schematic of predicted replication events using DNA fibers. **B–G**, Representative DNA fiber spreads and analysis of origin firing/stalled forks in human isogenic models of BRG1 loss (**B–F**) and overexpression (**E–G**). Green-red-green tracks indicative of new origins of replication are shown with yellow arrowheads. All data are mean  $\pm$  SD ( $n = 2–3$  for each cell line). **H** and **I**, Western blot analysis for prereplication proteins in human isogenic models of BRG1 loss and overexpression. KO, knockout; WT, wild-type.

Because BRG1 deficiency causes replication stress, we hypothesized that BRG1-containing SWI/SNF complexes may be engaged in protein interactions at forks to allow for efficient replication progression. To explore the proteome associated with SWI/SNF complexes in a defined system, we turned to our isogenic murine models. We performed coimmunoprecipitations (co-IP) in KP and KPB cells, using a core component of the complex, Baf47/Smardc1, as bait. Baf47 is part of two major classes of mammalian SWI/SNF complexes, canonical BAF (cBAF) and polybromo-associated BAF (PBAF), while the recently characterized noncanonical BAF (ncBAF) complexes were shown to lack Baf47 incorporation (3–8). We quantified the abundance of Baf47 protein interactors using quantitative mass spectrometry (Fig. 4A; Supplementary Table S4). Quantification of SWI/SNF subunit compositions showed that residual complexes in Brg1-deficient cells were enriched for subunits Brm, Ss18l1, Dpf2, and Smardc1. Mammalian SWI/SNF ATPase-dependent subunits including Ss18, Pbrm1, Actl6a, and Bcl7 were identified predominantly in Brg1 wild-type cells, as also shown by others (Supplementary Fig. S4A; ref. 63). Enrichment of Baf47 between KP and KPB cells was approximately equal with an overall fold change of  $-0.065$  (Fig. 4B). Compared with proteins enriched at the fork (64), proteins enriched in Brg1 wild-type cells were associated with the GO category prereplicative complex assembly (Fig. 4C). In Brg1-deficient cells, the top GO categories were associated with ssDNA repair and DNA damage response, consistent with our findings of increased RPA2 foci and presence of replication stress in human isogenic BRG1-deficient cells (Fig. 4C). The detection of known and expected interactions with Baf47 motivated us to look

further into tumor-specific interactions dependent on Brg1 expression in lung cancer cells, particularly those that functioned in the context of replication stress. Interestingly, Rpa1, the largest protein of the heterotrimeric RPA complex, and MCM-related proteins (Mcm6 and Mcm7) were strongly depleted in the Brg1-deficient setting (Fig. 4B; Supplementary Fig. S4A). Because the RPA heterotrimer is critical for the protection of ssDNA during physiologic DNA processes such as replication and repair, and has been shown to be involved in replication initiation and elongation (65, 66), we hypothesized that BRG1 might associate with the RPA complex during DNA replication.

We next used co-IP to test the idea that BRG1-containing SWI/SNF complexes associate with RPA complexes for fork progression and to prevent DNA breakage. Consistent with our hypothesis, we observed that RPA1 and RPA2 immunoprecipitated with BRG1 in human BRG1 wild-type cells (Fig. 4D; Supplementary Fig. S4B). In isogenic models of BRG1 loss, the interaction between the SWI/SNF complexes and RPA complex was lost (Fig. 4D). This suggested that the interaction between the two complexes is dependent on BRG1. Furthermore, BRG1 reconstitution restored these interactions, confirming they depend on intact BRG1 (Supplementary Fig. S4C). Interactions between BRG1-containing SWI/SNF complexes and RPA were also confirmed with antibodies against BAF47 and BAF170 in isogenic BRG1 contexts (Fig. 4E and F; Supplementary Fig. S4D and S4E). Co-IP also showed evidence for interactions between residual SWI/SNF complexes and ORC1, important for selecting replication origin sites (Supplementary Fig. S4F). These interactions were, however, found to be independent of BRG1. We were unable to detect any interactions

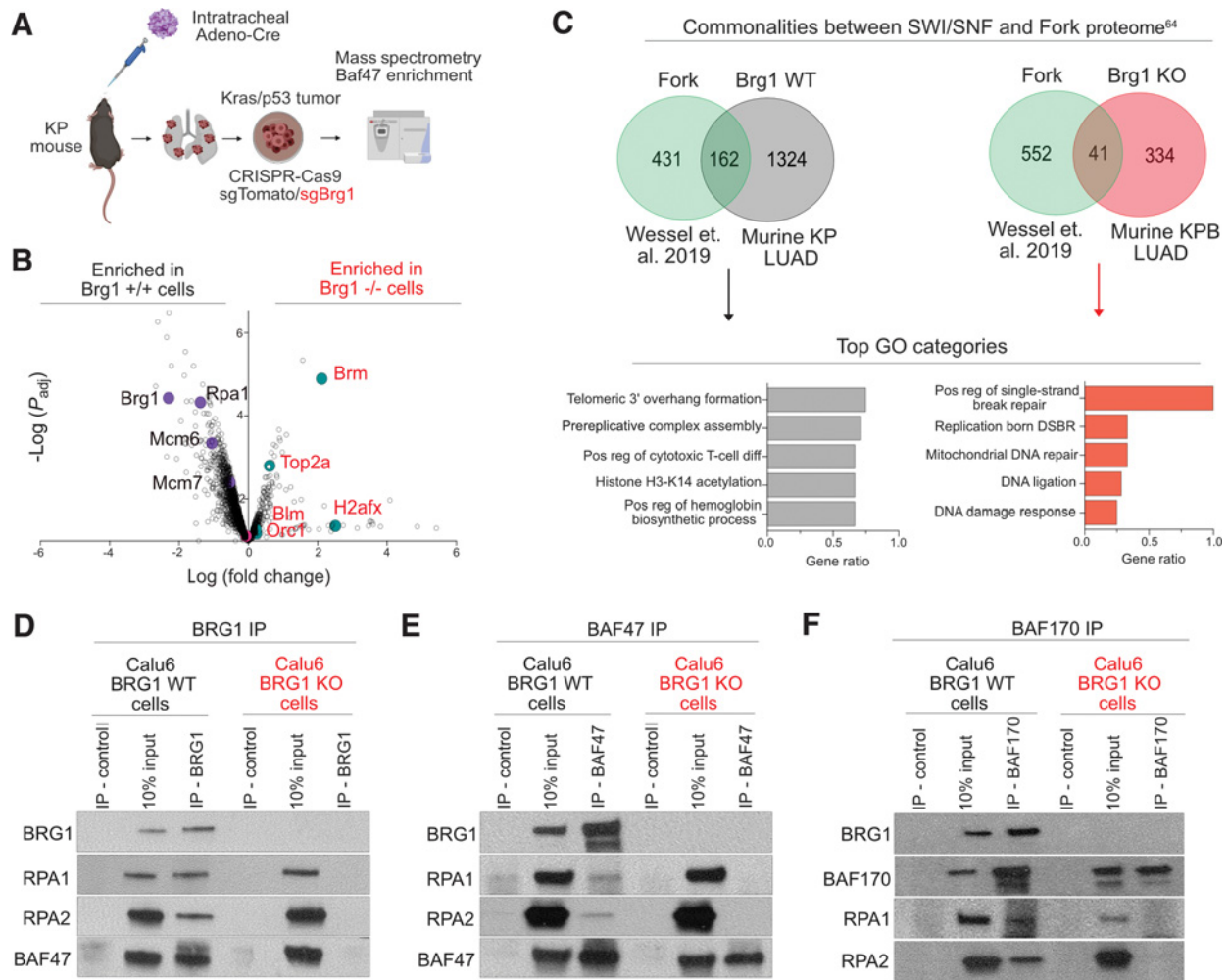


**Figure 4.**

Biochemical analysis of the mammalian SWI/SNF complex couples BRG1 with ongoing DNA replication via the RPA complex. **A**, Schematic of Baf47 co-IP performed in murine isogenic models of *Brg1* loss. **B**, Volcano plot depicting whole-proteome enrichment. Candidate proteins in each genotype are color coded [wild-type (WT), grape; knockout (KO), teal] on the basis of fold change (*x*-axis) and *P* value (*y*-axis). Baf47 was equally enriched in wild-type and knockout cells (pink dot). **C**, GO categories for proteins commonly identified between *Brg1* wild-type or knockout cells compared with fork-associated proteins. **D–F**, Co-IP experiments performed with antibodies against BRG1 (**D**), BAF47 (**E**), and BAF170 (**F**) in isogenic Calu6 models for RPA complexes. IP, immunoprecipitation; LUAD, lung adenocarcinoma.

between BRG1 and TOPBP1 (Supplementary Fig. S4G; ref. 21). Taken together, these findings suggest that BRG1-containing SWI/SNF complexes associate with ssDNA-bound RPA complexes and origin recognition protein ORC1, and loss of these interactions upon BRG1 loss could lead to defective fork progression.

Finally, we investigated whether the increased reliance on the ATR pathway in BRG1-deficient lung cancers could be exploited as a therapeutic vulnerability. We screened a set of small-molecule compounds targeted toward proteins involved in regulating aspects of DNA damage response and repair (Supplementary Fig. S5A). Isogenic BRG1-deficient cells were only sensitive to the treatment with either an ATR inhibitor (VX-970/M6620; ref. 67) or an inhibitor targeting its downstream effector kinase CHK1 (MK-8776; refs. 68, 69). The indistinguishable responses in viability between isogenic BRG1-proficient and -deficient cells to ATM or PARP inhibition suggested that the DNA repair responses were largely unaffected despite the absence of BRG1 in lung cancer cells (Supplementary Fig. S5A and S5B). Responses to aurora kinase A inhibitor, VX-680 (70), and CDK4/6 (71)

inhibitor, palbociclib, were also identical between BRG1-proficient and -deficient cells (Supplementary Fig. S5A and S5C). These experiments suggest that inhibition of the ATR pathway suppresses tumor growth in BRG1-deficient lung cancers by targeting the replication stress response.

We used several experimental systems to explore the ATR inhibitor sensitivity of BRG1-deficient lung cancer cells. Human BRG1-deficient cells showed a robust 3- to 6-fold higher sensitization to ATR inhibition compared with isogenic BRG1 wild-type cells, and reconstitution with BRG1 was able to restore this sensitivity back to control levels (Fig. 5A). Using a panel of human NSCLC cell lines, reduced values of VX-970 IC<sub>50</sub>s were observed in BRG1-mutant NSCLC cell lines, which predicted sensitivity to ATR inhibition (Supplementary Fig. S5D). Murine isogenic KP cells were 3- to 5-fold more sensitive to ATR inhibition (Fig. 5B). Further *in vitro* validation with cell lines derived from KRAS-mutant lung adenocarcinoma PDX models showed that BRG1 mutations were sufficient for a 7-fold reduction in cell viability upon treatment with ATR inhibitors (Fig. 5C). To

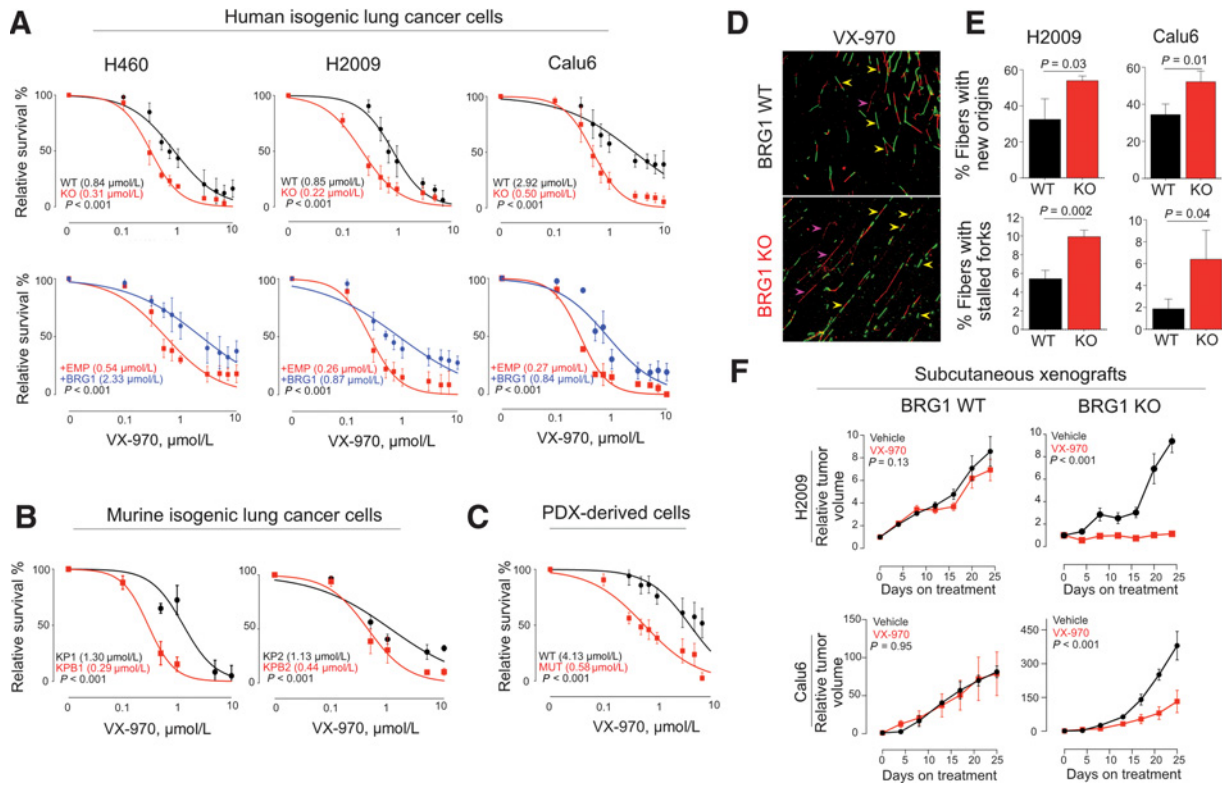


**Figure 5.**

*In vitro* and *in vivo* sensitivity of BRG1-mutant lung cancers to ATR inhibition. **A–C**, Relative survival in isogenic human BRG1 wild-type (WT), knockout (KO), and BRG1 reconstituted cells (**A**), murine isogenic models of Brg1 loss (**B**), and PDX models (**C**) after treatment with increasing doses of ATR inhibitor VX-970 performed for 72 hours using CellTiter Glo assays. All data points are relative to vehicle controls ( $n = 4–8$  for each human cell line,  $n = 3–5$  for each murine cell line, and  $n = 7$  for each PDX cell line). **D** and **E**, Representative images of DNA fiber spreads and analysis in human isogenic models of BRG1 loss after ATR inhibition. New origins of replication and fork stalls/collapse are indicated by yellow and pink arrowheads, respectively. All images are to scale and data are mean  $\pm$  SD ( $n = 3$  for each cell line). **F**, Subcutaneous tumor volumes of isogenic human BRG1 wild-type and knockout cells after treatment with vehicle or VX-970 for 25–30 days. Average tumor volume  $\pm$  SEM was measured every 4 days [H2009:  $n = 4$  (wild-type) and  $n = 3–5$  (knockout); and Calu6:  $n = 3$  (wild-type) and  $n = 4–6$  (knockout)]. Two-way ANOVA was performed to compute statistical significance.

determine whether additional replication stress could further enhance responses to ATR inhibition, we combined ATR inhibition with topoisomerase I inhibitor, irinotecan, to induce ssDNA breaks or hydroxyurea to cause deoxyribonucleotide depletion. Combinatorial treatment experiments further suppressed growth at nanomolar range concentrations of ATR inhibitors (Supplementary Fig. S5E and S5F). These findings demonstrate that loss of BRG1 creates a targetable dependence on the ATR pathway and the replication stress response in lung cancers.

We hypothesized that the replication dynamics in BRG1-deficient cells could be altered by the inhibition of ATR, given its role in replication stress responses. ATR inhibition further increased origin firing in BRG1-deficient cells and led to accumulation of stalled forks, as indicated through the presence single red track fibers (Fig. 5D and E). Single-molecule comet analysis of human isogenic cells treated with ATR inhibition revealed increased DNA breaks only in BRG1-deficient cells (Supplementary Fig. S5G–S5I). This suggests that ATR activation serves as an important molecular barrier to prevent further genomic instability to allow BRG1-deficient cancer cells to survive.

To investigate the therapeutic efficacy of targeting BRG1-deficient lung cancer cells with ATR inhibition *in vivo*, we transplanted human isogenic BRG1 wild-type and knockout cells subcutaneously into immunodeficient mice. Following the establishment of tumors, we

initiated treatment with either vehicle or VX-970. While BRG1 wild-type tumors exhibited no changes in tumor growth dynamics, BRG1-deficient tumors showed robust reductions in overall tumor size after treatment with ATR inhibition (Fig. 5F; Supplementary Fig. S5J).

Thus, *in vitro* and *in vivo* susceptibility of BRG1-deficient lung cancers to ATR inhibitors provides a possible therapeutic path based on defects in replication.

Finally, we wondered whether other cancers with BRG1 mutations behave similarly to lung cancers. Data from cancer datasets showed that mutation of BRG1 is also linked to other carcinoma types including endometrial (15%), stomach (8%), and rare ovarian cancers (100%; Supplementary Fig. S6A and S6B; ref. 72). Gene expression and pathway analysis confirmed a conserved replication stress response in other cancer types with BRG1 mutations (Supplementary Fig. S6C–S6E). An upregulated gene signature of 66 genes derived from patients with lung, endometrial, and stomach adenocarcinoma predicted poor prognosis in patients with lung adenocarcinoma (Supplementary Fig. S6F and S6G). Furthermore, analysis of synthetic lethality RNAi screening data from Project DRIVE (73) uncovered a high correlation between sensitivity to ATR knockdown and mutations in SWI/SNF ATPases BRG1/BRM across cancer cell lines representing different tissue types (Fig. 6A and B). While BRG1 was the predominant SWI/SNF ATPase mutated in all lines, BRM alone was mutated in

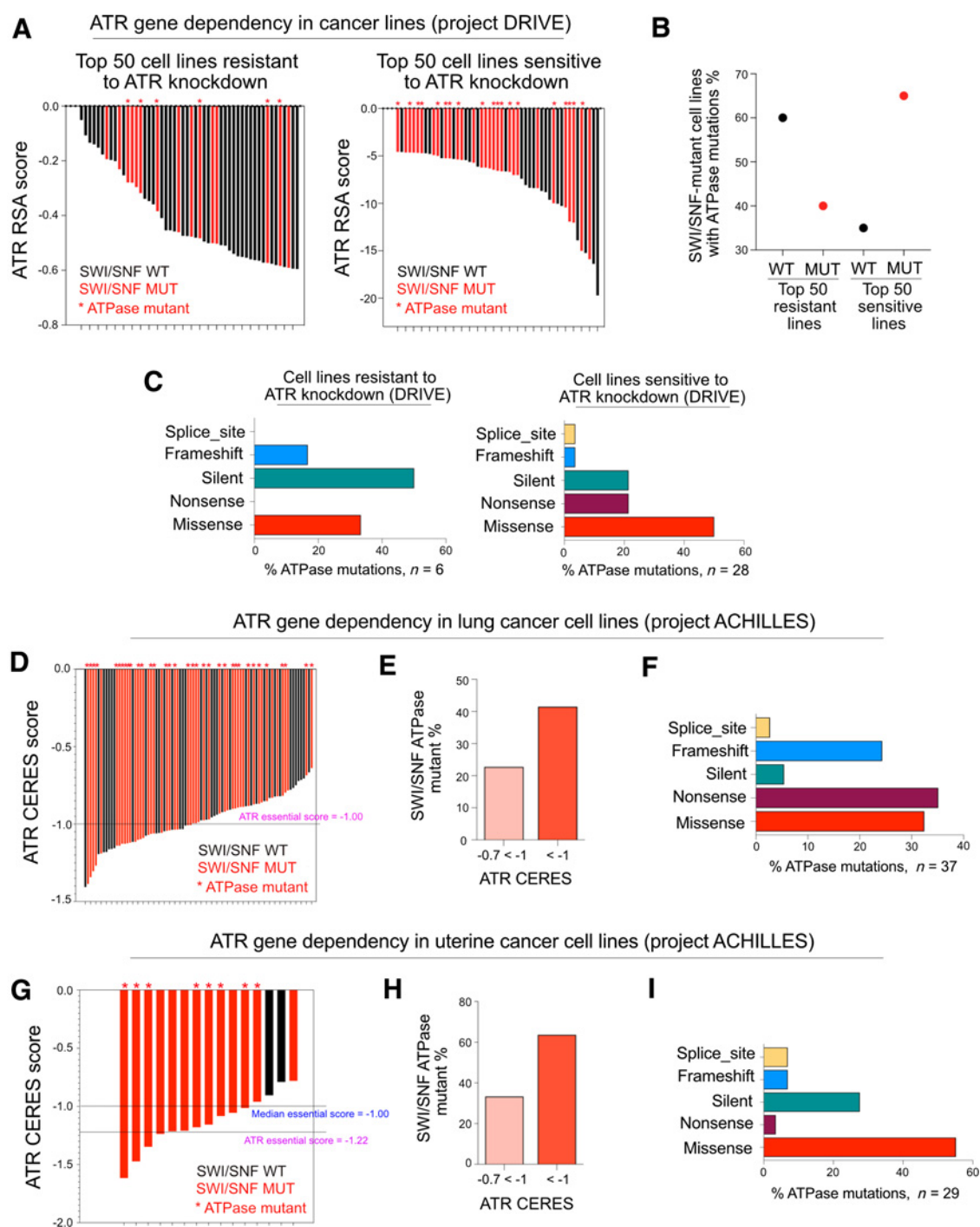


**Figure 6.**

Cancer dependency maps confirm synthetic lethal relationship between BRG1 and ATR. **A-C**, Analysis of siATR RSA scores from Project DRIVE. Types of ATPase mutations identified in cancer lines. **D-I**, Analysis of ATR knockout CERES scores from Project ACHILLES in lung (**D-F**) and uterine (**G-I**) cancer cell lines. ATR CERES ranges less than  $-0.7$  are depicted (lung, **E** and uterine, **H**). Thirty-seven SWI/SNF ATPase mutations (lung, **F**) and 29 (uterine, **I**) were identified in this analysis and have been grouped according to mutation type. MUT, mutant; WT, wild-type.

only four of 50 of most sensitive cell lines (Supplementary Table S5). Cancer cell lines with different kinds of *BRG1/BRM* mutations were found to be vulnerable to ATR knockdown (**Fig. 6C**). Interestingly, cell lines that had missense mutations, NCIH-1435 (lung), NCIH-2126

(lung), and NCIH-23 (lung), were among the most sensitive to ATR knockdown (Supplementary Table S5). These findings provide novel insight into the synthetic lethal relationship between BRG1 and ATR in lung as well as other cancer types with mutations in *BRG1*.

We corroborated these findings in CRISPR knockout screens using dependency data from Project ACHILLES (74, 75). We assessed ATR and BRG1 gene essentiality scores (CERES) in lung and uterine cancer cell lines. Among lung cancer lines with ATR CERES scores less than median gene essential score of  $-1$ , 40% of lung cell lines had mutations in *BRG1/BRM*, and 63% in uterine cancer lines (Fig. 6D–I; Supplementary Table S5). ATR was essential in cell lines bearing both missense and truncating mutations. These findings further support the conclusion that mutations in *BRG1* can predict ATR dependency.

## Discussion

This study provides novel insight for the role of *BRG1* and mammalian SWI/SNF complexes in lung cancer progression. We found that *BRG1* plays an important role in preventing replication stress and that *BRG1* may regulate origin firing in lung cancers. Our data suggest that *BRG1*-containing SWI/SNF complexes interact with ssDNA-binding protein RPA; thus, *BRG1* may impact the function of RPA at replication forks. Our data further suggest a link between SWI/SNF complex and ORC1, suggesting a potential role for *BRG1* in licensing or firing of origins. Knockout of *BRG1* in lung cancer isogenic models led to slowing of replication, induction of replication stress, increased origin firing, and activation of the ATR checkpoint pathway. The replication defects and the ATR dependence we observed provide a possible explanation for how lung cancer cells tolerate *BRG1* loss and survive in the presence of genome instability.

Our studies revealed novel potential protein interactions of SWI/SNF complexes that depend on *BRG1* in lung cancers. It is important to note that loss or mutation of *BRG1* in lung cancers may alter compositions of residual SWI/SNF complexes, such as cBAF, PBAF, and ncBAF; our study did not address this question. Further interrogation of how subcomplex identity affects replication stress responses will be important in future studies. We observed RPA complex interactions by co-IP with complex subunits *BRG1*, BAF47, and BAF170 in *BRG1* wild-type lung cancer cells. The RPA heterotrimer is linked to the protection of ssDNA during replication and also serves to recruit ATR/ATRIP during events of replication stress (52, 53). We speculate that loss of *BRG1* disrupts the binding of SWI/SNF and RPA, thereby allowing RPA to bind ssDNA at replication forks more efficiently. We suggest that this interaction leads to activation of ATR at stressed replication forks, creating a dependency on ATR to protect such forks. It is also likely that loss of *BRG1* promotes changes at the nucleosome accessibility level, which could in turn affect the replisome landscape (76). Thus, reduced interactions between SWI/SNF and RPA complexes and increased chromatin compaction could contribute to replicative stress and ATR dependence in *BRG1*-deficient lung cancer cells.

We hypothesize that loss of *BRG1* function leads to reduced fork speeds in lung cancer cells, providing an opportunity for increased origin firing to compensate for fork defects. We uncovered increased origin firing and increased CDC6 levels in *BRG1*-deficient lung cancer cells, consistent with this hypothesis. Firing of ongoing and dormant origins of replication is often an important compensatory mechanism to prevent fork stress-related defects from causing damage in cells (77, 78). The slowing or stalling of replication forks provides an opportunity for dormant origins to fire, which could also be assisted by the increased levels of CDC6 in *BRG1*-deficient cells. Elevation of origin firing in *BRG1*-deficient cells could also increase the number of replication forks slowed or stalled by compacted chromatin, increasing the consumption of dNTPs in cells and further promoting replication stress and genomic instability. This model could explain why *BRG1*

loss leads to a significant increase of replication stress and genomic instability in lung cancer. Thus, our data suggest that rather than simply promoting increased proliferation rates, mutations in *BRG1* may serve as a driving mechanism for advancing tumorigenesis by increasing genomic instability via a vis replicative stress.

Mutations in *BRG1* account for at least 10% of all NSCLC, with no currently approved precision medicine available for these patients. Clinicopathologic features of lung cancers have linked *BRG1* deficiency with primary resistance to standard treatments (14). Our results suggest that ATR activity is a critical barrier to prevent eventual mitotic catastrophe in *BRG1*-mutant lung cancers, revealing a new potential vulnerability for therapeutic targeting. Our findings show that loss of *BRG1* might be an important biomarker in patients with lung cancer that could benefit from ATR inhibition therapy. Interestingly, deletion of *ARID1A*, another member of the SWI/SNF complex, in colon cancer cells has been connected to sensitivity to ATR inhibitors (79). Of note, the lung cancer cell line, H460, used in this study, has an *ARID1A* mutation with undetectable levels of *ARID1A* protein. Deletion of *BRG1* in this *ARID1A*-mutant lung cancer background increased sensitivity to ATR inhibitors. Our data in lung cancer cells, combined with our analysis of ATR dependency screens in multiple cancer types, suggest that targeting ATR may represent a broad therapeutic strategy for patients with mutations in subunits of SWI/SNF complexes. ATR inhibitors are currently being tested in the clinic for other cancers (80). We suggest that it will be particularly fruitful to test ATR inhibition as therapy for patients with *BRG1*-mutant lung cancers and other *BRG1*-deficient cancers that exhibit replication stress responses.

## Disclosure of Potential Conflicts of Interest

C.P. Conception reports funding from American Cancer Society (postdoctoral fellowship) and Koch Institute (Quinquennial postdoctoral fellowship) during the conduct of the study. C.R. Stancliff reports grants from NCI Clinical Proteomic Tumor Analysis Consortium grants NIH/NCI U24-CA210986 during the conduct of the study. D.R. Mani reports grants from NCI (CPTAC #U24-CA210979) during the conduct of the study. A.T. Shaw reports personal fees from Novartis (employment, equity) outside the submitted work. A.N. Hata reports grants from Amgen, Pfizer, Relay Therapeutics, Roche/Genentech, Eli Lilly, Blueprint Therapeutics, and Novartis outside the submitted work. K.-K. Wong is an equity holder at G1 Therapeutics, Zentalis Therapeutics, and Epiphanies Therapeutics outside the submitted work. S.A. Carr reports grants from NIH/NCI during the conduct of the study, personal fees from Kymera and PTM Biolab, and Biogen (outside the submitted work), and non-financial support from Seer outside the submitted work. T. Jacks is a member of the board of directors of Amgen and Thermo Fisher Scientific, a co-founder of Dragonfly Therapeutics and T2 Biosystems, serves on the scientific advisory board of Dragonfly Therapeutics, SQZ Biotech, and Skyhawk Therapeutics; none of these affiliations represent a conflict of interest with respect to the design or execution of this study or interpretation of data presented in this article. T. Jacks also reports receiving funding from the Johnson & Johnson Lung Cancer Initiative and The Lustgarten Foundation for Pancreatic Cancer Research (outside the submitted work). C.F. Kim reports grants from NIH R01CA216188-01A1 (for project entitled “Mechanisms of Tumorigenesis in *Brg1* Mutant Lung Cancer”), American Cancer Society Mission Boost Grant for project entitled “Precision Therapy for SMARCA4-Mutant Lung Cancer,” reports consortium associations with Longfons Stichting and Celgene Corporation, and reports receiving funds from Genentech Inc., The Rockefeller University, and American Thoracic Society. No potential conflicts of interest were disclosed by the other authors.

## Authors' Contributions

**M. Gupta:** Conceptualization, formal analysis, investigation, writing-original draft, writing-review and editing. **C.P. Conception:** Conceptualization, resources, investigation. **C.G. Fahey:** Investigation. **H. Keshishian:** Data curation, formal analysis, methodology. **A. Bhutkar:** Data curation, formal analysis, methodology. **C.F. Brainson:** Investigation. **F.J. Sanchez-Rivera:** Investigation. **P. Pessina:** Investigation. **J.Y. Kim:** Investigation. **A. Simoneau:** Investigation. **M. Paschini:**

Investigation. **M.C. Beytagh:** Investigation. **C.R. Stanclift:** Investigation. **M. Schenone:** Investigation. **D.R. Mani:** Investigation. **C. Li:** Investigation. **A. Oh:** Investigation. **F. Li:** Investigation. **H. Hu:** Investigation. **A. Karatza:** Investigation. **R.T. Bronson:** Formal analysis, investigation. **A.T. Shaw:** Resources. **A.N. Hata:** conceptualization, resources. **K.-K. Wong:** Conceptualization, resources. **L. Zou:** Conceptualization, resources, formal analysis. **S.A. Carr:** conceptualization, resources, formal analysis. **T. Jacks:** Conceptualization, resources, supervision. **C.F. Kim:** Conceptualization, supervision, funding acquisition, project administration, writing-review and editing.

## Acknowledgments

We would like to thank members of the Kim Lab, Raul Mostoslavsky, Cigall Kadoch, Peter Sicinski, and Lynette Scholl for helpful discussions. M. Gupta was supported by the Albert J. Ryan graduate fellowship. C.P. Concepcion was supported by the American Cancer Society (ACS) postdoctoral fellowship 130361-PF-17-009-01-CDD and the Koch Institute (KI) Quinquennial Postdoctoral Fellowship. C.F. Brainson was supported by grants from the National Institute of General Medical Sciences P20-GM121327-03, NCI R01-CA237643, and the ACS Research Scholar

Grant 133123-RSG-19-081-01-TBG. Mass spectrometry/analysis was performed at the Broad Institute and was supported, in part, by grants from the NCI Clinical Proteomic Tumor Analysis Consortium grants NIH/NCI U24-CA210986 and NIH/NCI U01-CA214125 (to S.A. Carr) and NIH/NCI U24-CA210979 (to D.R. Mani). K.-K. Wong was funded by NCI R01-CA216188, R01-CA205150, and U01-CA213333. T. Jacks was supported by grants from Howard Hughes Medical Institute, Ludwig Center for Molecular Oncology at MIT, NIH P01 Jacks P01-CA42063, The Bridge Project, a partnership between the Koch Institute for Integrative Cancer Research at MIT and the Dana-Farber/Harvard Cancer Center (DF/HCC), and grants from the NCI KI Cancer Center Support Grant P30-CA14051. C.F. Kim was supported by NIH/NCI R01-CA216188, ACS Mission Boost Grant 71647, and DF/HCC Bridge Grant 72387.

The costs of publication of this article were defrayed in part by the payment of page charges. This article must therefore be hereby marked *advertisement* in accordance with 18 U.S.C. Section 1734 solely to indicate this fact.

Received May 27, 2020; revised June 15, 2020; accepted July 15, 2020; published first July 20, 2020.

## References

- Stewart BW, Wild CP. World cancer report 2014. Available at <https://publications.iarc.fr/Non-Series-Publications/World-Cancer-Reports/World-Cancer-Report-2014>.
- Cardarella S, Johnson BE. The impact of genomic changes on treatment of lung cancer. *Am J Respir Crit Care Med* 2013;188:770–5.
- Kadoch C, Crabtree GR. Mammalian SWI/SNF chromatin remodeling complexes and cancer: mechanistic insights gained from human genomics. *Sci Adv* 2015;1:e1500447.
- Wilson BG, Roberts CW. SWI/SNF nucleosome remodellers and cancer. *Nat Rev Cancer* 2011;11:481–92.
- Michel BC, D'Avino AR, Cassel SH, Mashtalir N, McKenzie ZM, McBride MJ, et al. A non-canonical SWI/SNF complex is a synthetic lethal target in cancers driven by BAF complex perturbation. *Nat Cell Biol* 2018;20:141–20.
- Alpsoy A, Dykhuizen EC. Glioma tumor suppressor candidate region gene 1 (GLTSCR1) and its paralog GLTSCR1-like form SWI/SNF chromatin remodeling subcomplexes. *J Biol Chem* 2018;293:3892–903.
- Gatchalian J, Malik S, Ho J, Lee D-S, Kelso TWR, Shokhiev MN, et al. A non-canonical BRD9-containing BAF chromatin remodeling complex regulates naive pluripotency in mouse embryonic stem cells. *Nat Commun* 2018;9:5139.
- Wang X, Wang S, Troisi EC, Howard TP, Haswell JR, Wolf BK, et al. BRD9 defines a SWI/SNF sub-complex and constitutes a specific vulnerability in malignant rhabdoid tumors. *Nat Commun* 2019;10:1881.
- Wong AK, Shanahan F, Chen Y, Lian L, Ha P, Hendricks K, et al. BRG1, a component of the SWI-SNF complex, is mutated in multiple human tumor cell lines. *Cancer Res* 2000;60:6171–7.
- Reisman DN, Sciarrotta J, Wang W, Funkhouser WK, Weissman BE. Loss of BRG1/BRM in human lung cancer cell lines and primary lung cancers: correlation with poor prognosis 1. *Cancer Res* 2003;63:560–6.
- Medina PP, Romero OA, Kohno T, Montuenga LM, Pio R, Yokota J, et al. Frequent BRG1/SMARCA4-inactivating mutations in human lung cancer cell lines. *Hum Mutat* 2008;29:617–22.
- Rodriguez-Nieto S, Cañada A, Pros E, Pinto AI, Torres-Lanzas J, Lopez-Rios F, et al. Massive parallel DNA pyrosequencing analysis of the tumor suppressor BRG1/SMARCA4 in lung primary tumors. *Hum Mutat* 2011;32:E1999–2017.
- Rodriguez-Nieto S, Sanchez-Cespedes M. BRG1 and LKB1: tales of two tumor suppressor genes on chromosome 19p and lung cancer. *Carcinogenesis* 2009;30:547–54.
- Dagogo-Jack I, Schrock AB, Kem M, Jessop N, Lee J, Ali SM, et al. Clinicopathologic characteristics of BRG1-deficient NSCLC. *J Thorac Oncol* 2020;15:766–76.
- Bultman S, Gebuhr T, Yee D, La Mantia C, Nicholson J, Gilliam A, et al. A Brg1 null mutation in the mouse reveals functional differences among mammalian SWI/SNF complexes. *Mol Cell* 2000;6:1287–95.
- Glaros S, Cirrincione GM, Palanca A, Metzger D, Reisman D. Targeted knockout of BRG1 potentiates lung cancer development. *Cancer Res* 2008;68:3689–96.
- Marquez-Vilendrer SB, Rai SK, Gramling SJ, Lu L, Reisman DN. Loss of the SWI/SNF ATPase subunits BRM and BRG1 drives lung cancer development. *Oncoscience* 2016;3:322–36.
- Chung W-J, Daemen A, Cheng JH, Long JE, Cooper JE, Wang B-E, et al. Kras mutant genetically engineered mouse models of human cancers are genomically heterogeneous. *Proc Natl Acad Sci U S A* 2017;114:E10947–55.
- Dykhuizen EC, Hargreaves DC, Miller EL, Cui K, Korshunov A, Kool M, et al. BAF complexes facilitate decatenation of DNA by topoisomerase II $\alpha$ . *Nature* 2013;497:624–7.
- Bourgo RJ, Siddiqui H, Fox S, Solomon D, Sansam CG, Yaniv M, et al. SWI/SNF deficiency results in aberrant chromatin organization, mitotic failure, and diminished proliferative capacity. *Mol Biol Cell* 2009;20:3192–99.
- Cohen SM, Chastain PD, Rosson GB, Groh BS, Weissman BE, Kaufman DG, et al. BRG1 co-localizes with DNA replication factors and is required for efficient replication fork progression. *Nucleic Acids Res* 2010;38:6906–19.
- Dunaief JL, Strober BE, Guha S, Khavari PA, Álin K, Luban J, et al. The retinoblastoma protein and BRG1 form a complex and cooperate to induce cell cycle arrest. *Cell* 1994;79:119–30.
- Dimitrova N, Gocheva V, Bhutkar A, Resnick R, Jong RM, Miller KM, et al. Stromal expression of miR-143/145 promotes neoangiogenesis in lung cancer development. *Cancer Discov* 2016;6:188–201.
- Ran FA, Hsu PD, Wright J, Agarwala V, Scott DA, Zhang F. Genome engineering using the CRISPR-Cas9 system. *Nat Protoc* 2013;8:2281–308.
- Sánchez-Rivera FJ, Papagiannakopoulos T, Romero R, Tammela T, Bauer MR, Bhutkar A, et al. Rapid modelling of cooperating genetic events in cancer through somatic genome editing. *Nature* 2014;516:428–31.
- Shalem O, Sanjana NE, Hartenian E, Shi X, Scott DA, Mikkelsen TS, et al. Genome-scale CRISPR-Cas9 knockout screening in human cells. *Science* 2014;343:84–7.
- Fillmore CM, Gupta PB, Rudnick JA, Caballero S, Keller PJ, Lander ES, et al. Estrogen expands breast cancer stem-like cells through paracrine FGF/Tbx3 signaling. *Proc Natl Acad Sci U S A* 2010;107:21737–42.
- Xi Q, He W, Zhang XH, Le HV, Massagué J. Genome-wide impact of the BRG1 SWI/SNF chromatin remodeler on the transforming growth factor beta transcriptional program. *J Biol Chem* 2008;283:1146–55.
- Zacharek SJ, Fillmore CM, Lau AN, Gludish DW, Chou A, Ho JWK, et al. Lung stem cell self-renewal relies on bmi1-dependent control of expression at imprinted loci. *Cell Stem Cell* 2010;9:272–81.
- Fillmore CM, Xu C, Desai PT, Berry JM, Rowbotham SP, Lin Y-J, et al. EZH2 inhibition sensitizes BRG1 and EGFR mutant lung tumours to TopoII inhibitors. *Nature* 2015;520:239–42.
- Li B, Dewey CN. RSEM: accurate transcript quantification from RNA-seq data with or without a reference genome. *BMC Bioinformatics* 2011;12:323.
- Langmead B, Trapnell C, Pop M, Salzberg SL. Ultrafast and memory-efficient alignment of short DNA sequences to the human genome. *Genome Biol* 2009;10:R25.
- Leng N, Dawson JA, Thomson JA, Ruotti V, Rissman AI, Smits BMG, et al. EBSeq: an empirical Bayes hierarchical model for inference in RNA-seq experiments. *Bioinformatics* 2013;29:1035–43.
- Anders S, Huber W. Differential expression analysis for sequence count data. *Genome Biol* 2010;11:R106.

35. Bult CJ, Blake JA, Smith CL, Kadin JA, Richardson JE, Anagnostopoulos A, et al. Mouse genome database (MGD) 2019. *Nucleic Acids Res* 2019;47: 801–6.
36. Subramanian A, Tamayo P, Mootha VK, Mukherjee S, Ebert BL, Gillette MA, et al. Gene set enrichment analysis: a knowledge-based approach for interpreting genome-wide expression profiles. *PNAS* 2005;102:15545–50.
37. Liberzon A, Birger C, Thorvaldsdóttir H, Ghandi M, Mesirov JP, Tamayo P. The molecular signatures database (MSigDB) hallmark gene set collection. *Cell Syst* 2015;1:417–25.
38. Györfy B, Surowiak P, Budczies J, Lanczky A. Online survival analysis software to assess the prognostic value of biomarkers using transcriptomic data in non-small-cell lung cancer. *PLoS One* 2013;8:e82241.
39. Nieminiusz J, Schwab RA, Niedzwiedz W. The DNA fibre technique – tracking helicases at work. *Methods* 2016;108:92–8.
40. Li J, Han S, Li H, Udeshi ND, Svinkina T, Mani DR, et al. Cell-surface proteomic profiling in the fly brain uncovers wiring regulators. *Cell* 2020;180:373–86.
41. Cerami E, Gao J, Dogrusoz U, Gross BE, Sumer SO, Aksoy BA, et al. The cBio cancer genomics portal: an open platform for exploring multidimensional cancer genomics data. *Cancer Discov* 2012;2:401–4.
42. Gao J, Aksoy BA, Dogrusoz U, Dresdner G, Gross B, Sumer SO, et al. Integrative analysis of complex cancer genomics and clinical profiles using the cBioPortal. *Sci Signal* 2013;6:p11.
43. Mi H, Muruganujan A, Thomas PD. PANTHER in 2013: modeling the evolution of gene function, and other gene attributes, in the context of phylogenetic trees. *Nucleic Acids Res* 2013;41:D377–86.
44. Thomas PD, Campbell MJ, Kejariwal A, Mi H, Karlak B, Daverman R, et al. PANTHER: a library of protein families and subfamilies indexed by function. *Genome Res* 2003;13:2129–41.
45. Cai L, Lin S, Girard L, Zhou Y, Yang L, Ci B, et al. LCE: an open web portal to explore gene expression and clinical associations in lung cancer. *Oncogene* 2019; 38:2551–64.
46. Cancer Genome Atlas Research Network; Collisson EA, Campbell JD, Brooks AN, Berger AH, Lee W, et al. Comprehensive molecular profiling of lung adenocarcinoma: The Cancer Genome Atlas Research Network. *Nature* 2014; 511:543–50.
47. Hoadley KA, Yau C, Hinoue T, Wolf DM, Lazar AJ, Drill E, et al. Cell-of-origin patterns dominate the molecular classification of 10,000 tumors from 33 types of cancer. *Cell* 2018;173:291–304.
48. DuPage M, Dooley AL, Jacks T. Conditional mouse lung cancer models using adenoviral or lentiviral delivery of Cre recombinase. *Nat Protoc* 2009;4: 1064–72.
49. Jackson EL, Olive KP, Tuveson DA, Bronson R, Crowley D, Brown M, et al. The differential effects of mutant p53 alleles on advanced murine lung cancer. *Cancer Res* 2005;65:10280–8.
50. Kavanaugh G, Ye F, Mohni KN, Luzwick JW, Glick G, Cortez D. A whole genome RNAi screen identifies replication stress response genes. *DNA Repair* 2015;35: 55–62.
51. Papillon JPN, Nakajima K, Adair CD, Hempel J, Jouk AO, Karki RG, et al. Discovery of orally active inhibitors of brahma homolog (BRM)/SMARCA2 ATPase activity for the treatment of brahma related gene 1 (BRG1)/SMARCA4-mutant cancers. *J Med Chem* 2018;61:10155–72.
52. Gaillard H, García-Muse T, Aguilera A. Replication stress and cancer. *Nat Rev Cancer* 2015;15:276–80.
53. Yazinski SA, Zou L. Functions, regulation, and therapeutic implications of the ATR checkpoint pathway. *Annu Rev Genet* 2016;50:155–73.
54. Bensimon A, Simon A, Chiffaudel A, Croquette V, Heslot F, Bensimon D. Alignment and sensitive detection of DNA by a moving interface. *Science* 1994; 265:2096–8.
55. Merrick CJ, Jackson D, Diffley JF. X. Visualization of altered replication dynamics after DNA damage in human cells. *J Biol Chem* 2004;279: 20067–75.
56. Maya-Mendoza A, Moudry P, Merchut-Maya JM, Lee M, Strauss R, Bartek J. High speed of fork progression induces DNA replication stress and genomic instability. *Nature* 2018;559:279–84.
57. Pereira PD, Serra-Caetano A, Cabrita M, Bekman E, Braga J, Rino J, et al. Quantification of cell cycle kinetics by EdU (5-ethynyl-2'-deoxyuridine)-coupled-fluorescence-intensity analysis. *Oncotarget* 2017;8:40514–32.
58. Imielinski M, Berger AH, Hammerman PS, Hernandez B, Pugh TJ, Hodis E, et al. Mapping the hallmarks of lung adenocarcinoma with massively parallel sequencing. *Cell* 2012;150:1107–20.
59. Zehir A, Benayed R, Shah RH, Syed A, Middha S, Kim HR, et al. Mutational landscape of metastatic cancer revealed from prospective clinical sequencing of 10,000 patients. *Nat Med* 2017;23:703–13.
60. Bell SP, Dutta A. DNA replication in eukaryotic cells. *Annu Rev Biochem* 2002; 71:333–74.
61. Diffley JFX. Regulation of early events in chromosome replication. *Curr Biol* 2004;14:R778–86.
62. Neelsen KJ, Zanini IMY, Mijic S, Herrador R, Zellweger R, Ray Chaudhuri A, et al. Deregulated origin licensing leads to chromosomal breaks by rereplication of a gapped DNA template. *Genes Dev* 2013;27:2537–42.
63. Pan J, McKenzie ZM, D'Avino AR, Mashtalir N, Lareau CA, St. Pierre R, et al. The ATPase module of mammalian SWI/SNF family complexes mediates subcomplex identity and catalytic activity-independent genomic targeting. *Nat Genet* 2019;51:618–26.
64. Wessel SR, Mohni KN, Luzwick JW, Dungrawala H, Cortez D. Functional analysis of the replication fork proteome identifies BET proteins as PCNA regulators. *Cell Rep* 2019;28:3497–509.
65. Fairman MP, Stillman B. Cellular factors required for multiple stages of SV40 DNA replication *in vitro*. *EMBO J* 1988;7:1211–8.
66. Zou Y, Liu Y, Wu X, Shell SM. Functions of human replication protein A (RPA): from DNA replication to DNA damage and stress responses. *J Cell Physiol* 2006; 208:267–73.
67. Knegtel R, Charrier JD, Durrant S, Davis C, O'Donnell M, Storck P, et al. Rational design of 5-(4-(isopropylsulfonyl)phenyl)-3-(4-((methylamino)methyl)phenyl)isoxazol-5-yl)pyrazin-2-amine (VX-970, M6620): optimization of intra- and intermolecular polar interactions of a new ataxia telangiectasia mutated and rad3-related (ATR) kinase inhibitor. *J Med Chem* 2019;62:5547–61.
68. Dwyer MP, Paruch K, Labroli M, Alvarez C, Keertikar KM, Poker C, et al. Discovery of pyrazolo[1,5-a]pyrimidine-based CHK1 inhibitors: a template-based approach—part 1. *Bioorg Med Chem Lett* 2011;21:467–70.
69. Labroli M, Paruch K, Dwyer MP, Alvarez C, Keertikar K, Poker C, et al. Discovery of pyrazolo[1,5-a]pyrimidine-based CHK1 inhibitors: a template-based approach—part 2. *Bioorg Med Chem Lett* 2011;21:471–4.
70. Tagal V, Wei S, Zhang W, Brekken RA, Posner BA, Peyton M, et al. SMARCA4-inactivating mutations increase sensitivity to Aurora kinase A inhibitor VX-680 in non-small cell lung cancers. *Nat Commun* 2017;8:14098.
71. Xue Y, Meehan B, Fu Z, Wang XQD, Fiset PO, Rieker R, et al. SMARCA4 loss is synthetic lethal with CDK4/6 inhibition in non-small cell lung cancer. *Nat Commun* 2019;10:557.
72. Jelinic P, Mueller JJ, Olvera N, Dao F, Scott SN, Shah R, et al. Recurrent SMARCA4 mutations in small cell carcinoma of the ovary. *Nat Genet* 2014; 46:424–6.
73. McDonald ER, de Weck A, Schlabach MR, Billy E, Mavrakis KJ, Hoffman GR, et al. Project DRIVE: a compendium of cancer dependencies and synthetic lethal relationships uncovered by large-scale, deep RNAi screening. *Cell* 2017;170: 577–92.
74. Meyers RM, Bryan JG, McFarland JM, Weir BA, Sizemore AE, Xu H, et al. Computational correction of copy number effect improves specificity of CRISPR-Cas9 essentiality screens in cancer cells. *Nat Genet* 2017;49:1779–84.
75. Tsherniak A, Vazquez F, Montgomery PG, Weir BA, Kryukov G, Cowley GS, et al. Defining a cancer dependency map. *Cell* 2017;170:564–76.
76. Azmi IF, Watanabe S, Maloney MF, Kang S, Belsky JA, MacAlpine DM, et al. Nucleosomes influence multiple steps during replication initiation. *Elife* 2019;6: e22512.
77. Brambati A, Zardoni L, Achar YJ, Piccini D, Galanti L, Colosio A, et al. Dormant origins and fork protection mechanisms rescue sister forks arrested by transcription. *Nucleic Acids Res* 2018;46:1227–39.
78. Alver RC, Chadha GS, Blow JJ. The contribution of dormant origins to genome stability: from cell biology to human genetics. *DNA Repair* 2014;19:182–9.
79. Williamson CT, Miller R, Pemberton HN, Jones SE, Campbell J, Konde A, et al. ATR inhibitors as a synthetic lethal therapy for tumours deficient in ARID1A. *Nat Commun* 2016;7:13837.
80. Lecona E, Fernandez-Capetillo O. Targeting ATR in cancer. *Nat Rev Cancer* 2018;18:586–95.